ZULFAQAR Journal of Defence Science, Engineering & Technology
e-ISSN: 2773-5281
Vol. 4, Issue 2 (2021)
DOI: https://doi.org/10.58247/jdset-2021-0402-15
Journal homepage: https://zulfaqarjdset.upnm.edu.my

STRUCTURAL ANALYSIS OF BULKHEAD PATCH REPAIR DUE TO HEAT DAMAGE

Hasif Yahaya[a,b], Gunasilan Manar[b*]

[a] Royal Malaysian Air Force, Butterworth Air Base, Butterworth, Penang, Malaysia
[b] Department of Mechanical Engineering, Faculty of Engineering, National Defence University of Malaysia, Sungai Besi Camp, 57000 Kuala Lumpur, Malaysia

ARTICLE INFO

ARTICLE HISTORY
Received: 19-05-2021
Received: 10-08-2021
Accepted: 03-09-2021
Published: 31-12-2021

KEYWORDS
Aluminium alloy stainless steel
Heat damage
Structural patch repair

ABSTRACT

The integrity of the aircraft structure after a permanent repair requires thorough engineering analysis. In this study, the aircraft's defective Bulkhead was damaged due to heat exposure and repaired with a patching technique known as a bulkhead patch repair. The study aimed to analyse the repair carried out using numerical calculation and finite element analysis. The first result of the numerical calculation shows that the repair part (stainless steel) will restore the original part (AA7050) strength capability. The second result from the LS-Dyna analysis shows that heat damage had caused the material (AA7050) strength to deteriorate significantly. The final loads testing using LS-Dyna analysis on components shows the patch repair scheme conducted could strengthen the damaged part by transferring the applied loads to repair part. The outcome of this study justified that for better maintenance action (structural integrity consideration), the damaged Y453 Bulkhead needed to be replaced instead of conducting permanent repair.

1.0 INTRODUCTION

Service life damage is a normal condition happening to the aircraft structure, compromising safety, and integrity [1]. Service life is defined as the duration of the aircraft usage starting from the aircraft's turnover from the manufacturer to the airliner or military services until the retirement of the aircraft. During that time, the aircraft's defects are categorized as a structural defect, avionics defect, engine defect, and system defect. The maintenance crew would repair these defects on regular occasions, but there is a requirement to seek advice from the respective division or authority in severe cases. The structural defects show the highest types of cases representing 55% of total cases [2].

Common materials used in the fuselage production include aluminium alloy, titanium alloy, and steel [3]. Aluminium alloys are widely use on the aircraft structure because of their high strength to weight ratio. The alloy consists of two or more metals, which can increase the materials' strength according to the requirement with desirable weight. Aluminium alloy is well known as high-performance material, established design process, cost-effectiveness, and availability of raw materials and manufacturing facilities [4]. F/A-18's bulkhead's main components starting from forward to aft are known as Y453, Y470.5, and Y488 bulkheads, see Figure 1. The bulkheads are made from 7050-T7451 aluminium alloy thick section plate machined to size accordingly and coated with anti-corrosion material [5].

*Corresponding Author | Manar, G. | gunasilan@upnm.edu.my

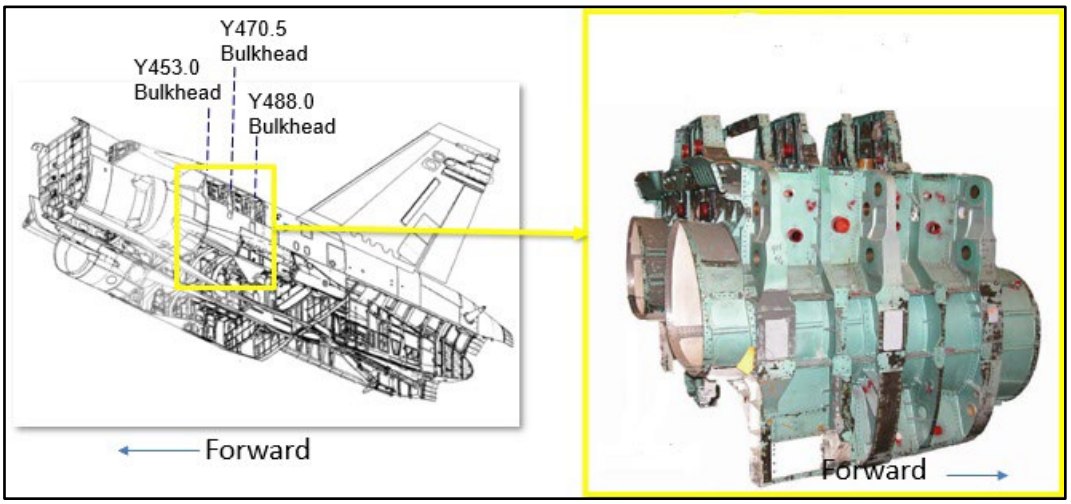

Figure 1. Y453 bulkhead [5]

Types of structural defects happening on the aircraft structure can be categorized into five (5) main types: elongated holes, crack, impact, corrosion, and overheating [2]. In this paper, the focus is on the overheat impact on the structure. The structure overheating is the structure's exposure to a specific elevated temperature for a particular time, thus causing structural damage. The temperature effect strongly influences the strength of the material. Pure aluminium without any alloying elements has a melting and boiling temperature at around 655°C and 2425°C respectively [6]. Aluminium alloys have a melting temperature varying based on the alloying element. In terms of mechanical properties, most aluminium alloys show a reduction in strength after 150 °C to 200°C.

In a comparative study done on the variety of aluminium alloy material, there was a drop of 90% of the material's tensile strength when exposed to temperature elevated from room temperature till 370°C for 0.5-hour exposure [7]. This effect will reduce the operational capability of the component. Figure2 shows the impact on heat damage based on discoloration. The effect of temperature on the aluminium structure will reduce the structure's operational capability by softening strain hardened and redistributing local stress in creep [8]. Creep is defined as a process of material deform permanently due to mechanical stress [9]. It occurs due to a high level of stress but still below the yield strength of the materials. For example, when subjected to heat for a long period, creep always increase with temperature increases. Stages of creep can be divided into three developments [10-11]; primary creep, which happens at a fast rate, secondary creep, which occurs at a steady pace and tertiary creep happens rapidly and rupture to failure. The author also mentioned that the creep generally happened at 30% to 40% of the materials melting temperature. For records, the melting temperature of aluminium alloy is in the range of 475 °C to 675 °C.

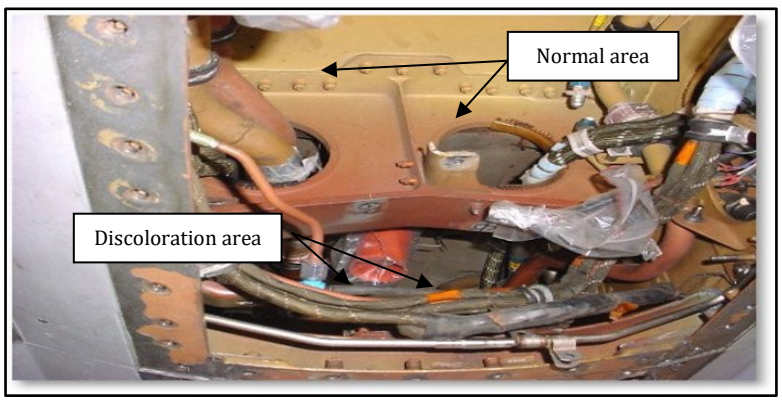

Figure 2. Heat damage on AA7075 Y453 bulkhead

*Corresponding Author | Manar, G. | gunasilan@upnm.edu.my

2.0 METHODOLOGY

2.1 Mechanical Properties

Based on the Metallic Materials Properties Development and Standardization (MMPDS), the mechanical properties of the AA7050 and stainless steel are shown in Table 1.

Table 1. Mechanical properties [12]

Properties	Aluminium alloy 7050	Stainless steel
Ultimate Stress	510.2 MPa	1068.69 MPa
Yield Stress	441.264 MPa	999.74 MPa

For the simulation conducted with the highest accuracy, the use of material thermal properties is compulsory. The thermomechanical properties include thermal conductivity, specific heat, density, thermal expansion coefficient, and elasticity modulus, as shown in Table 2.

Table 2. Thermomechanical properties of AA7050 [13]

Property	Measurement
Temperature	371℃
Density	2746.6 kg. m^{-3}
Specific heat	1012.4 J. $(kg. K)^{-1}$
Thermal conductivity	151.9 W. $(m. K)^{-1}$
Coefficient of thermal expansion	30.37$(10^{-5})K^{-1}$
Young modulus	57.29GPa

2.2 Model Geometry

Using the manual calculation, the load-carrying capability of the original part (AA7050) was defined and then compared with the repair part (Stainless Steel) using stress analysis beyond specification method [14]. The numerical analysis was conducted to decide whether the repair part will restore the damaged material's original load-carrying capability. Figure 3 and Figure4 show the 3D computer-aided design (CAD) model of affected bulkhead structure (AA7050) and patching structure (stainless steel), respectively.

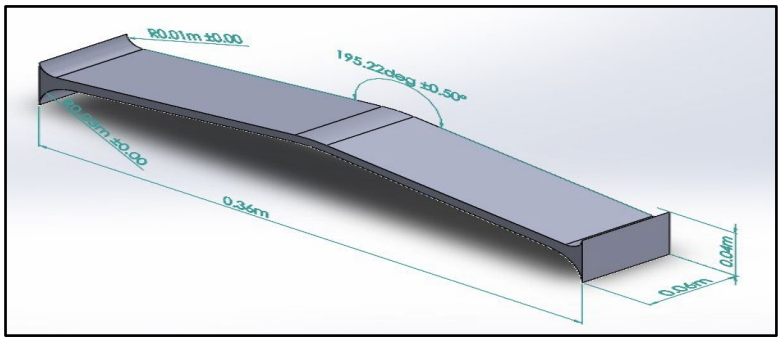

Figure 3. Isometric view of AA7050 part

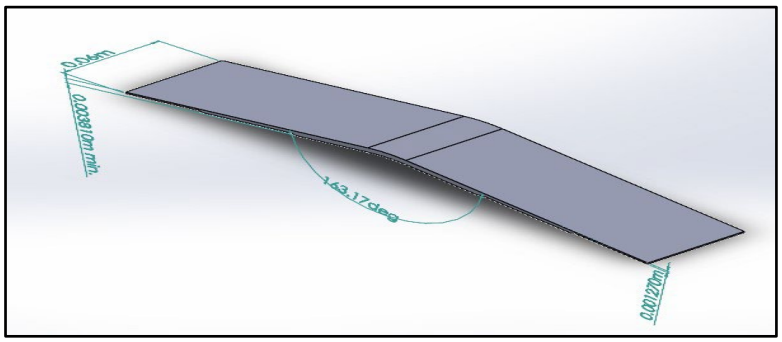

Figure 4. Isometric view of stainless steel

*Corresponding Author | Manar, G. | gunasilan@upnm.edu.my

2.3 Simulation Setup

Based on the CAD models, the simulations were performed using the CAE software, LS-Dyna. Simulations were performed by heating the AA7050. The types of keywords used for thermal analysis were MAT_004_ELASTIC_PLASTIC_THERMAL and T01_THERMAL_ISOTROPIC because the temperature dependant coefficient materials and thermal isotropic are individually defined.

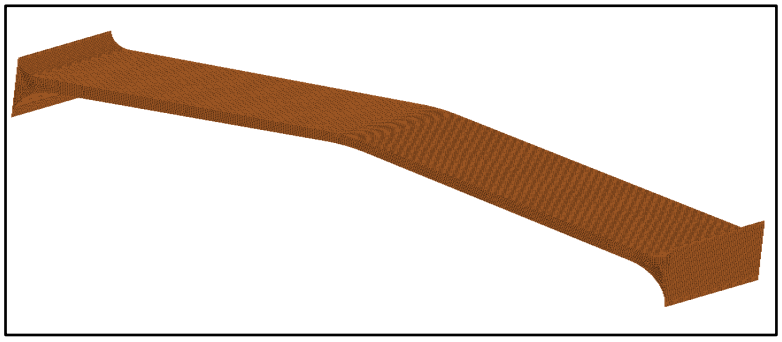

Figure 5. Mesh model generation AA7050 part

Figure 5 shows the model mesh which consists of 172,149 elements. The second type of simulations was then performed using axial x-axis load 40kN on the original structure and structure at elevated temperature [15]. The resultant stress produced by thermal analysis was applied as pre-stress for the damaged part - the stress created by using the keyword INTERFACE_SPRINGBACK_LSDYNA. The output in the dynain file (the file that contain keyword data) was used again to run the second simulation on the damaged part. Figure 6 shows the combined structure and exploded view of the meshing details. Different from the original structure that used hexahedron mesh elements, the repair part used tetrahedron meshing. This is because, the model of both parts has different angles and dimension variation.

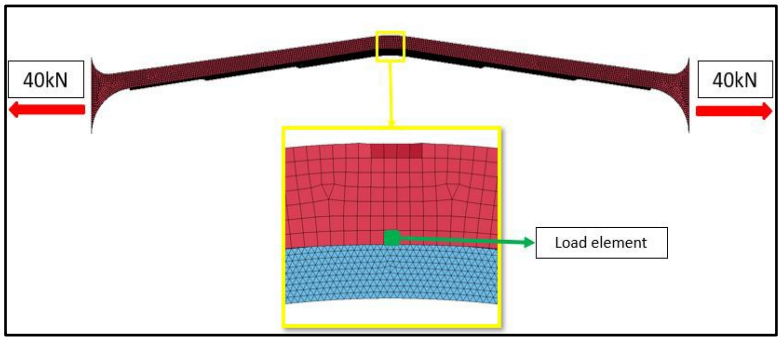

Figure 6. Load Direction and element location

There are two types of analysis conducted in this research. The first analysis is the temperature effects analysis on the original structure (AA7050). For the first analysis, the temperature effects, all the original structure nodes were heated from 30°C (room temperature) till 371°C (the maximum value of leak air) for maximum effects. The effects in terms of resultant displacement and effective stress (Von-Misses stress) were then analysed.

The second analysis is the loading effect analysis. It was done by comparing the original structure's effects without heat damage, the original structure after heat damage, and the assembly structure. The axial loading of 40kN was applied on both sides of the structure to simulate tension stress on the structure as per Figure 6. The force was chosen as per experimental works conducted on crotch region Y470 Bulkhead [16-17]. It was mentioned earlier, there are three steps of analysis on different conditions and assembly of parts. The result of the elongation and displacement was compared for each of the conditions.

*Corresponding Author | Manar, G. | gunasilan@upnm.edu.my

2.4 Model Validation

In order to validate the overall simulation based on experimental result, the same scale of parts dimension need to be fabricated and conducted the said testing via experiment. This study only relies on the input by the material properties and conducting the simulations. Thus, one way to validate the simulation is by comparing the deformation of material in the simulation with the real experimental data representing by stress-strain curve. The graph in Figure 7 shows two stress-strain curve graphs of material simulations (red curve) and actual material (blue curve). Both curves were identical to each other, showing that the displacement effects before the stress applied were the same as the actual material data based on the simulation analysis.

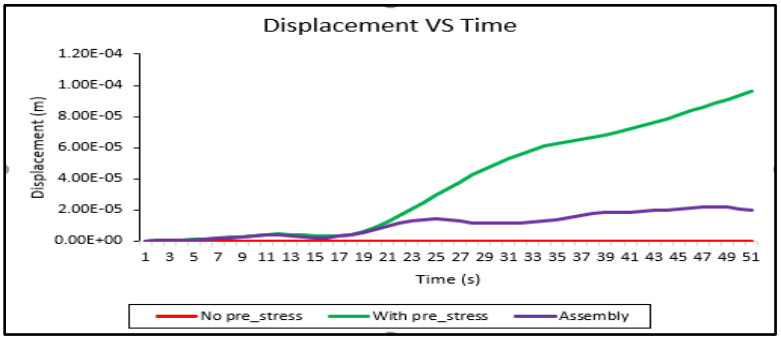

Figure 7. Comparison of stress-strain curve between simulation and actual values from MMPDS

3.0 RESULT AND DISCUSSIONS

3.1 Numerical Analysis

Both AA7050 and Stainless-steel parts showed equal value of the material load-carrying capability of 1,280,100 kg and 1,275,192 kg, respectively. The percentage of the difference between the results of the load-carrying ability was just 0.33%. Thus, with the repair part's size, it could handle all the loads impacting the damaged structure, the same as the original capability. The sample of calculation for numerical analysis is shown below:

Sample calculation AA7050:

Ultimate stress, Ftu	= 510 Mpa
Yield stress, Fty	= 441 Mpa x 1.5 = 661.5 Mpa
Design ultimate allowable, Fdu	= Less (Ftu or 1.5xFty) = 510 Mpa
Warea	= ½ x (9.14+6.86) x 157 x 2 = 2510 mm^2
Load capability, Pcap	= 510 Mpa x $2510^{-6}m^2$= 130,571.1 kg

3.2 Heat Damage Simulation Result

The effects of the elevated temperature on the original structure of AA7050 using the simulation are shown in Figure 8. This condition can be compared with the actual condition in Figure 9. The obvious effect was that the real structure was having discolouration and so as the simulation result. This can be defined as the depletion of strength due to elevated temperature.

*Corresponding Author | Manar, G. | gunasilan@upnm.edu.my

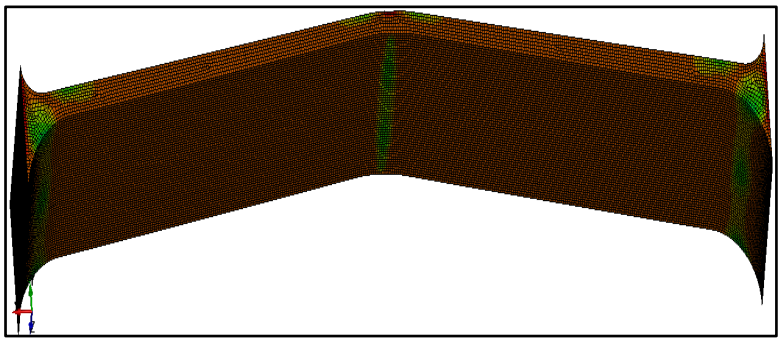

Figure 8. Heat damage simulation result

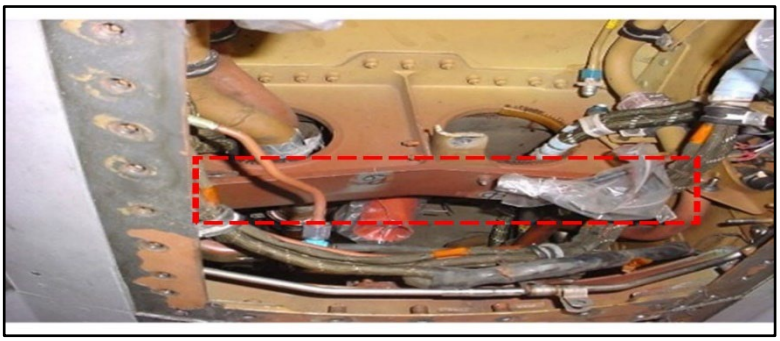

Figure 9. Actual condition

The highest stress was recorded on the areas of fix joints, whereas the heat effect had caused repel force due to fix conditions. The highest effective stress (Von-Mises Stress) recorded as shown in Figure 10 is σvm = 539.5 MPa, while the yield strength of the material was only σy = 441.3 MPa. Thus, the material of original structure (AA7050) had failed due to σvm higher than σy (σvm >σy). The expansion due to heat on original structure is about 0.38 mm in horizontal direction as shown in Figure 11.

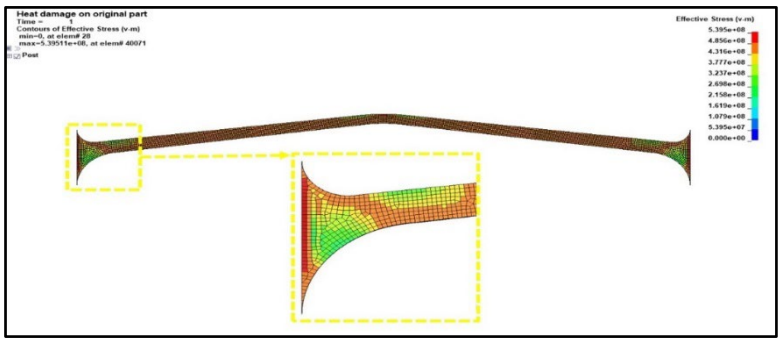

Figure 10. Heat effects on effective stress

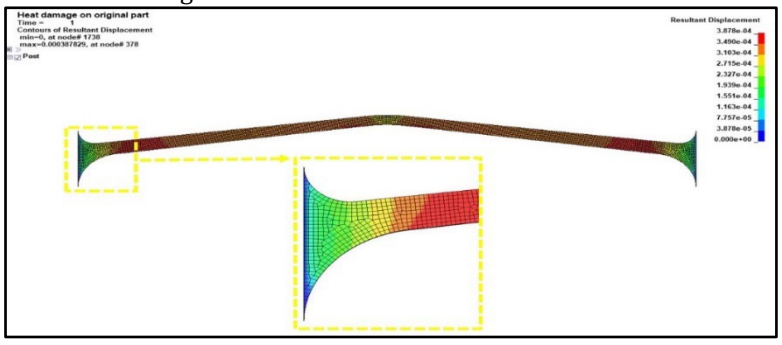

Figure 11. Heat effects on resultant displacement

*Corresponding Author | Manar, G. | gunasilan@upnm.edu.my

3.3 Estimation On Tensile Strength After Heat Damage

The outcome of the simulation does not directly show the strength of the affected structure. The resultant strength can be defined using an experiment by estimation from the graph of the effect of exposure at the elevated temperature [11]. The graph in Figure 12 shows the estimate tensile strength left after the heat damage. Based on graph extrapolation of 371 C effects, the strength was just 21% of the actual tensile strength. Thus, in this case the actual tensile strength was σt = 510.2 MPa, then if only 21% of the tensile strength left, the strength of the AA7050 after heat damage will be σt_new = 102.04 MPa.

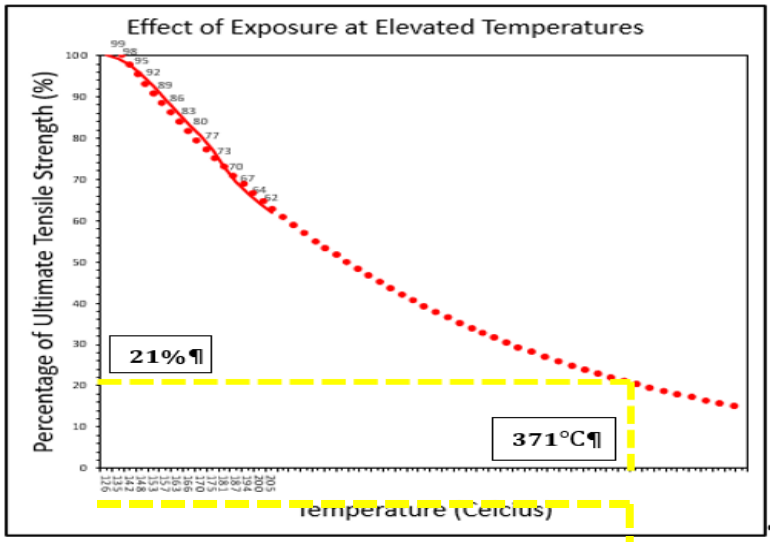

Figure 12. Effect of exposure on elevated temperature [11]

3.4 Loading Analysis Simulation Result

Figure 13 shows the displacement effect on the original structure without heat damage (no pre-stress). In comparison, Figure 14 shows the displacement effect on the original structure after heat damage (with pre-stress). Figure 15 shows the displacement of the damaged structure attached to the repair part (assembly part).

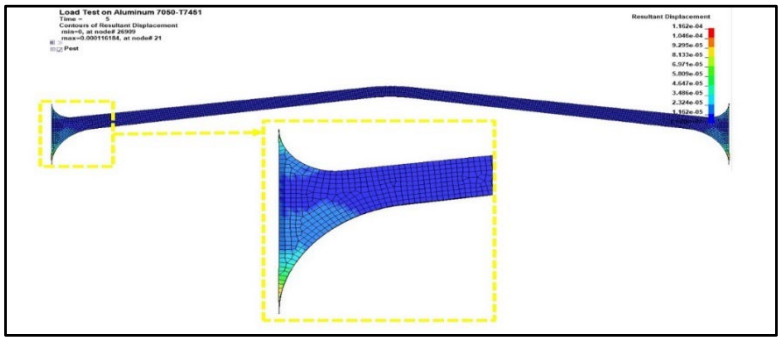

Figure 13. Without pre-stress

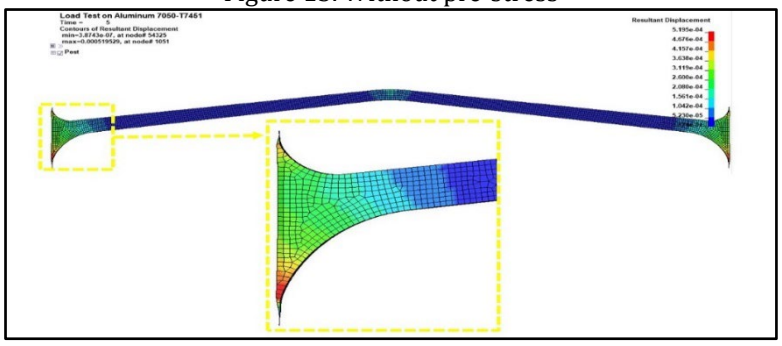

Figure 14. With pre-stress

*Corresponding Author | Manar, G. | gunasilan@upnm.edu.my

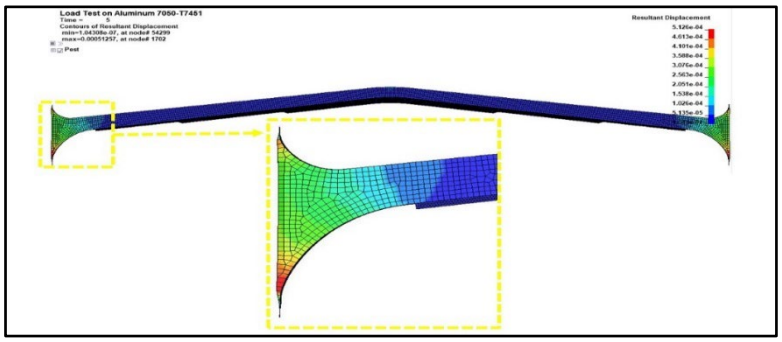

Figure 15. Assembly part

The maximum displacement due to loading effects applied to three types of structure is shown in Table 3. It is based on the element location mentioned in the previous section. While Figure 16 shows the three types of graphs, the red graph (no pre-stress) represents the original part without heat damage, the green graph (with pre-stress) illustrates the original part with heat damage, and the purple graph represents the original part with heat damage being attached with repair part.

Table 3. Maximum displacement effects

Part conditions	Displacement
Without pre stress	0 meter
With pre stress	9.60×10^{-5} meter
Assembly part	2.20×10^{-5} meter

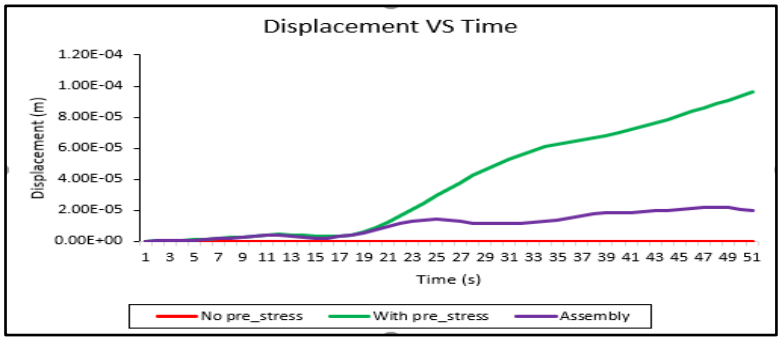

Figure 16. Displacement vs time for the structure

As per Figure 16, the red graph was steady with zero displacement, due to the load applied of 40kN could not cause any displacement to the original part. Then on the green graph, the displacement incremental was the highest when used with the same load, as the material's strength had been depleted to absorb the same load. And lastly, with an additional attachment of the repair part to the damaged part, on the purple graph, the displacement incremental was lower than the green graph but still showed deformation. This can be explained that the damaged structure is transferring the load to the repair part, thus reducing the displacement effects.

4.0 CONCLUSION

The research had complied with all the listed research objectives. At first, both parts had an equal value of material load-carrying capability of 1,280,100 kg and 1,275,192 kg, respectively. Thus, the repaired part could restore the original part's ability. Secondly, the simulation result shows that maximum Von-Mises stress (539.5 MPa) exceeded the tensile yield strength (441.3 MPa); thus, the original part had failed due to heat damage. Lastly, the axial loads' graph shows that the assembly part's displacement was lower than the damaged part because the applied loads were transferred to the repair part. This study may be used as a pre-analysis since this research is conducted based on simulations only. The simulation needs to be properly validated by experimental works. The only feasible validation in this study is by using stress-strain curve material deformation. In the study's overall recommendations based on structural integrity criteria, for the best maintenance action on Y453 Bulkhead damage, the structural replacement needs to

*Corresponding Author | Manar, G. | gunasilan@upnm.edu.my

be carried out. This is based on the facts that the repair assembly shows capability degradation in the same applied load and creep deformation is already happening on the structure.

5.0 ACKNOWLEDGEMENT

The authors fully acknowledged Ministry of Higher Education (MOHE) and National Defence University of Malaysia (NDUM) for the approved fund which makes this research feasible.

List of Reference

[1] Umamaheswar, T. V., & Singh, R. (1999). Modelling of a patch repair to a thin cracked sheet. Engineering Fracture Mechanics, 62(2-3), 267-289.
[2] Chen, C., & Li, K. (2020). Design and stress analysis for aircraft structure repair beyond specification. In Proceedings of the International Conference on Aerospace System Science and Engineering 2019 (pp. 253-264). Springer Singapore.
[3] Fielding, J. P. (1994, September). Graduate aircraft design education. In ICAS PROCEEDINGS (Vol. 19, pp. 1866-1866). AMERICAN INST OF AERONAUTICS AND ASTRONAUTICS.
[4] Manar, G., & Longère, P. (2019). Crack arrest capabilities of AA2024 and AA7175 aluminium alloys under impact loading. Engineering Failure Analysis, 104, 1107-1132.
[5] Barter, S., & Dixon, B. (2009). Investigation using quantitative fractography of an unexpected failure in an F/A-18 centre fuselage bulkhead in the FINAL teardown program. Engineering Failure Analysis, 16(3), 833-848.
[6] Kaufman, J. G. (2000). Introduction to aluminium alloys and tempers. ASM international.
[7] Huda, Z., Zaharinie, T., & Min, G. J. (2010). Temperature effects on material behavior of aerospace aluminum alloys for subsonic and supersonic aircraft. Journal of Aerospace Engineering, 23(2), 124-128.
[8] Heath-Smith, J. R., & Kiddle, F. E. (1975). Effects of heat on fatigue in aircraft structure.
[9] Singh, S. B., Ranjan, P., & Haghi, A. K. (2022). Materials Modeling for Macro to Micro/nano Scale Systems. Apple Academic Press.
[10] Norizan, Y. N. A., Din, M. F. M., Zamri, W. F. H. W., Hashim, F. R., Jusoh, M. T., & Rahman, M. R. A. (2018, February). The effects of different heat treatment annealing on structural properties of LaFe11. 5Si1. 5 compounds. In AIP Conference Proceedings (Vol. 1930, No. 1). AIP Publishing.
[11] Din, M. F., Wang, J. L., Norizan, Y. N. A., Shamba, P., Hashim, F. R., Idris, N. H., & Zamri, W. F. H. (2018, September). Systematically study on the magnetism and critical behaviour of layered NdMn1. 4Cu0. 6Si2. In AIP Conference Proceedings (Vol. 2016, No. 1). AIP Publishing.
[12] Rice, R. C., Jackson, J. L., Bakuckas, J., & Thompson, S. (2003). Metallic materials properties development and standardization. MMPDS). National Technical Information Service, cap, 1-4.
[13] Yanpu, C., Lehua, Q., & Zhengmin, B. (2016). 3D dynamic simulation analysis of thermal-mechanical coupling during 7075 aluminum alloy micro-droplet deposition manufacture. Rare Metal Materials and Engineering, 45(8), 1924-1930.
[14] Chen, C., & Li, K. (2020). Design and stress analysis for aircraft structure repair beyond specification. In Proceedings of the International Conference on Aerospace System Science and Engineering 2019 (pp. 253-264). Springer Singapore.
[15] Bartholomeusz, R. A., Baker, A. A., Chester, R. J., & Searl, A. (1999). Bonded joints with through-thickness adhesive stresses–reinforcing the F/A-18 Y470. 5 bulkhead. International journal of adhesion and adhesives, 19(2-3), 173-180.
[16] Bartholomeusz, R. A., & Searl, A. (2002). Case History: Bonded Composite Reinforcement of the F/A-18 Y470. 5 Centre Fuselage Bulkhead. In Advances in the Bonded Composite Repair of Metallic Aircraft Structure (pp. 859-870). Elsevier Science Ltd.
[17] Ya'acob, W. M. H. W., Razali, N. A. M., Jasni, A. H., Rusdi, R. A. A., Salleh, E. M., & Halim, N. A. (2019). Optimising the mixing factor condition of natural cellulose/epoxy composite by using response surface method. Zulfaqar Journal of Defence Science, Engineering & Technology, 2(2).

*Corresponding Author | Manar, G. | gunasilan@upnm.edu.my